FULL PAPER

3D-printed open-source sensor flow cells for microfluidic temperature, electrical conductivity, and pH value determination

Robin Dinter[1] · Lennart Helwes[1] · Stijn de Vries[1] · Kausik Jegatheeswaran[1] · Henning Jibben[1] · Norbert Kockmann[1]

Abstract

Due to the miniaturization of equipment for flow chemistry and microprocess engineering, low-cost sensors and analytical devices are becoming increasingly important for automated inline process control and monitoring. The combination of 3D printing technology and open-source lab automation facilitates the creation of a microfluidic toolbox containing tailored actuators and sensors for flow chemistry, enabling a flexible and adaptable design and efficient processing and control based on the measured data. This contribution presents a set of 3D-printed microfluidic sensor flow cells for inline measurement of temperature, electrical conductivity (EC), and pH value, while compensating for the temperature dependence of EC and pH. The tailored sensor flow cells were tested using model reactions in a single-phase capillary flow system. They have an accuracy comparable to reference sensors in batch measurements. The sensor data can be used to monitor the reaction progress (conversion), determine the kinetic data (activation energy, pre-exponential factors) of saponification reactions, and identify titration characteristics (equivalence and isoelectric points) of neutralization reactions. Hence, the 3D-printed microfluidic sensor flow cells offer an attractive alternative to commercial analytical flow devices for open-source and low-cost lab automation.

Keywords Inline measurement · Flow cell · Flow analysis · Electrical conductivity (EC) · pH value · Saponification · Neutralization

Introduction

The demand for miniaturized, robust, and low-cost analytical flow sensors that can be used for automated process control, monitoring and determining reaction parameters is rising due to the advanced progress of miniaturization in microprocess engineering and flow chemistry [1–3]. The use of microfluidic equipment in the transfer from batch to flow chemistry has the advantage of improving process intensification, overall efficiency, throughput, and heat and mass transfer due to the large specific surface-to-volume ratio [4, 5]. Miniaturized actuators and sensors are required for qualitative and quantitative analysis of microfluidic flow [6]. Optical, ultrasonic, and capacitance-based sensors are already available to measure velocities, concentrations, phase proportions, and conductivities [1, 2, 7–9]. Unfortunately, many commercially available analytical flow devices are costly, proprietary, and not adaptable or flexible to microfluidic requirements and specifications [10, 11]. Therefore, utilizing 3D printing technology for manufacturing microfluidic devices and do-it-yourself lab-ware is an emerging trend [4, 5, 12].

There are two main methods for producing 3D-printed objects, used in this contribution. In the first method, a heated thermoplastic filament is extruded through a small nozzle to build up layers and create the object [12]. The second method uses a photopolymerizing process, called stereolithography (SL), to cure and solidify a resin and solidify it into a hardened object [1, 12]. This allows for faster iteration of prototypes than conventional subtractive methods and low manufacturing costs, resulting in tailored and highly accurate microfluidic devices [12, 13]. By combining 3D printing

✉ Robin Dinter
   robin.dinter@tu-dortmund.de

✉ Norbert Kockmann
   norbert.kockmann@tu-dortmund.de

1   Department of Biochemical and Chemical Engineering,
    Laboratory of Equipment Design, TU Dortmund University,
    Emil-Figge-Str. 68, 44227 Dortmund, Germany

with physical computing using open-source hardware and software, an independent toolbox of low-budget and tailored sensors and actuators for flow chemistry can be created where each sensor or actuator can be used independently of the others [1, 13–16]. These two advanced technologies help to extend the boundaries of open-source microfluidic lab automation and create flexible and tailored analytical devices.

For the design and manufacturing of 3D-printed sensor flow cells for microfluidic monitoring, it is essential to distinguish between invasive (inline) and non-invasive (online) measurement techniques [1, 8, 17, 18]. The first example is a conductometer, which measures the electrical conductivity (EC) to monitor and quantify the ion concentration of a solution. In the invasive (inline) measurement technique for EC in batch mode, two electrodes are immersed directly in an electrolyte solution [19]. In contrast, a non-invasive (online) technique has been introduced by Zemann *et al.* [20] and Fracassi da Silva *et al.* [21] using a capacitively coupled contactless conductivity sensor (C4D) with two cylindrical electrodes outside of the capillary measuring in flow mode. Due to its design, the sensor requires a special signal processing circuit, which increases the cost [7, 20, 21]. A second example is a potentiometer that measures pH values to monitor and quantify the acidity or basicity of a solution. The most straightforward technique for measuring pH uses a glass membrane immersed directly into the analyte solution [22], while an advanced optical method employs the reflection of light varying with the pH of the liquid, which needs optical access to the fluid but does not need to be in contact with the solution [23–25].

The aim of this study was to develop a set of tailored microfluidic sensor flow cells that in-line measure temperature, EC, and pH value. The flow cells were manufactured using subtractive and additive manufacturing techniques and included open-source lab automation devices. As model system, the saponification and neutralization reactions were conducted in a single-phase capillary flow system to validate the effectiveness of these self-build and cost-effective microfluidic sensor flow cells compared to reference batch measurements. Based on the measured data, the reaction progress was calculated and monitored, the reaction parameters (conversions, activation energies, pre-exponential factors) were determined, and titration characteristics (equivalence and isoelectric points) were identified.

Measurement principles

In Fig. 1A, B, an overview of the measurement principles for EC and pH value is shown, which are required for the subsequent design and construction of the sensor flow cells for measuring characteristic reaction parameters and titration points. In addition, the experimental setup and the automation strategy (Fig. 1C, D) are introduced.

Electrical conductivity (EC) and conductometry

In order to determine the EC, a method was utilized that involved placing two electrodes in an electrolyte solution and applying an alternating voltage (AC) as an excitation signal (Fig. 1A). This method is called conductometry and is based on the fact that the EC of a solution is proportional to the concentration of ions in the solution [26]. The electrical resistance of the electrolyte solution is determined by measuring the impedance [10, 27–30]. The schematic structure of an EC sensor is shown together with the equivalent circuit diagram in Fig. 1A. The measured impedance indirectly represents the electrical conductance G, as explained in the ESI Section 1. This allows the derivation of the EC κ by combining the electrical conductance G with the cell constant K, as expressed in Eq. 1 [26, 31]:

$$\kappa = G \cdot K = G \cdot \frac{l}{A} \tag{1}$$

The cell constant K of the sensor flow cell is a sensor-specific value and the quotient of the electrode distance l and the electrode surface A, and is selected to be 1 cm^{-1} for the most common applications [26, 31]. In order to compare ECs measured at different temperatures, the measurements are standardized to a reference temperature of 25 °C, as explained in more detail in ESI Section 1.

pH value and potentiometry

The acidity or basicity of a solution is determined by its pH value and the strength of an acid or base by its pK_A value [22, 32, 33]. Additional information on the acid-base theory and the pH scale can be found in the literature [22, 32, 33]. The pH value is measured without knowing the concentration and strength of the substances by using an electrometric measurement method called potentiometry or potentiometric cell. This method uses a voltmeter to measure the potential difference between two electrodes immersed in an analyte solution [22]. The reference electrode has fixed potential and on the other hand, the measuring electrode uses an ion-selective glass membrane [22, 34], as shown in Fig. 1B. The measured voltage is then converted into the pH value using the modified Nernst Equation S5 according to the ESI Section 2.

Experimental setup and automation strategy

The experimental single-phase flow setup in sa coiled capillary reactor made of fluoroethylene propylene (FEP) is explained in ESI Section 3.1 for measuring the temperature-compensated EC (Fig. 1C) or pH value (Fig. 1D).
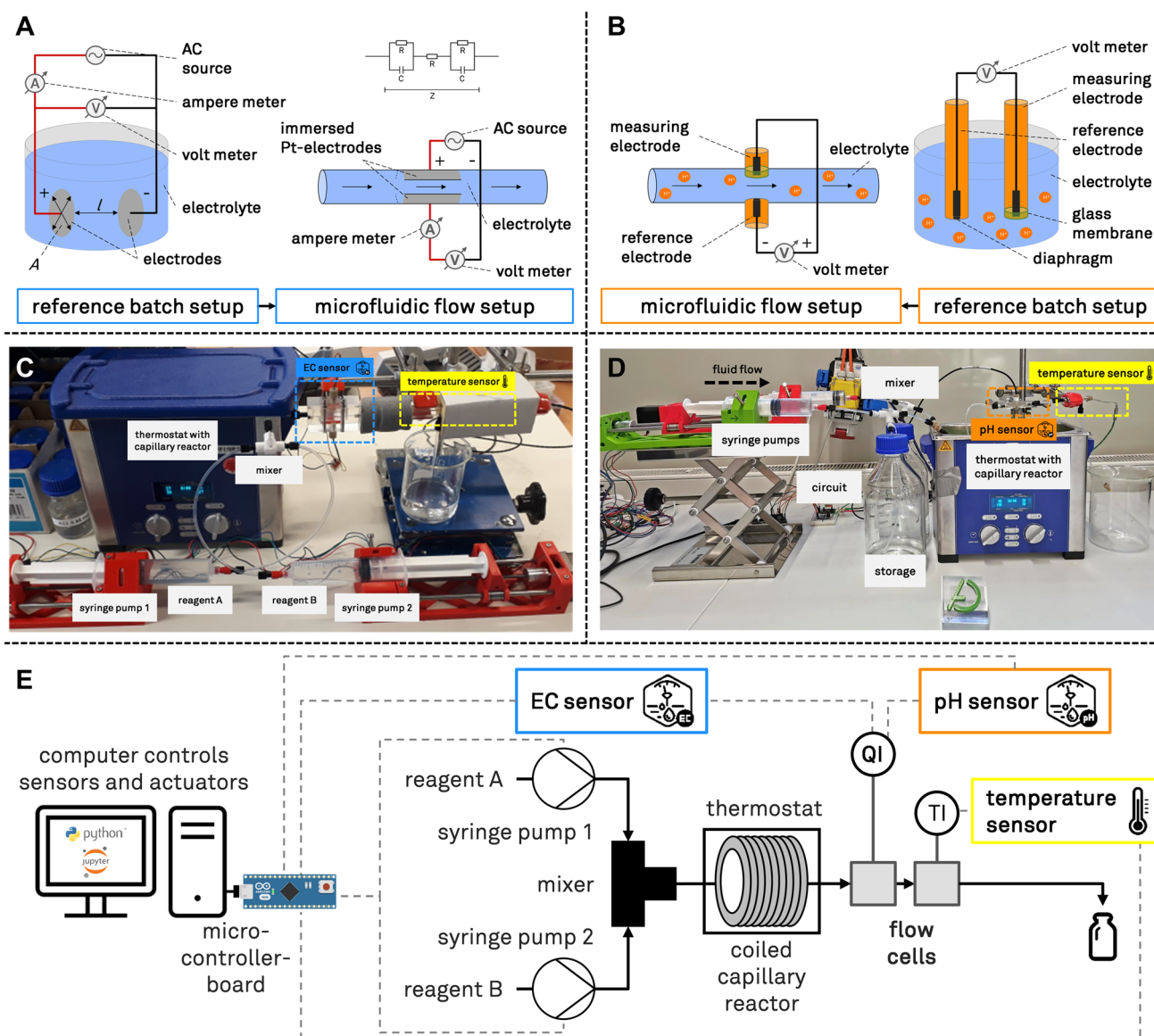
Fig. 1 Measuring principles of a conductometer (**A**) and a potentiometer (**B**) in batch and flow chemistry. Laboratory experimental flow setup, including flow generation, coiled capillary reactor, and tailored flow cells for measuring temperature-compensated electrical conductivity (**C**) or pH value (**D**). Schematic setup of the automation strategy using open-source microcontroller and breakout boards (**E**)

In addition, the corresponding reference batch setup is given in ESI Section 3.2. An open-source lab automation strategy for the flow setup was implemented, as displayed in Fig. 1E. All actuators and sensors were connected to a computer managed by Python and Arduino scripts, as explained in the ESI Section 4 and in a GitHub repository. The microcontroller-board (MCB) is responsible for communicating with the sensors, displaying the measured data, handling the calibration protocol, and controlling the volumetric flow rates of the open-source syringe pumps [35] based on temperature-compensated flow measurements.

Results and discussion

The aim of this study was to develop a series of tailored microfluidic sensor flow cells that measure temperature, EC, and pH inline. To this end, flow cells were constructed using subtractive and additive manufacturing techniques ("Construction of sensor flow cells" Section) and verified in ESI Section 6. Subsequently, the validated microfluidic sensor flow cells were applied with the saponification and neutralization model reactions (ESI Section 5) using the experimental flow setup

with open-source laboratory automation ("Experimental setup and automation strategy" Section) to investigate the application range.

Construction of sensor flow cells

First, a compilation of the three sensor flow cells developed and manufactured to measure temperature (A), EC (B), and pH (C) in the microchannel are shown in Fig. 2 and explained in the following. The SL 3D printer Formlabs Form 3+ was used for additive manufacturing. The accuracy and precision of these sensor flow cells are evaluated against commercial reference devices in ESI Section 6 to determine the overall performance of the customized microfluidic flow cells.

Temperature measurement

Due to the temperature dependence of the EC and pH value, a temperature sensor flow cell was constructed in parallel for compensation. The temperature sensor consists of a Pt100 resistance thermometer (Pt100A 10/10, Electronic Sensor, Heilbronn, Germany) immersed in a flow cell (Fig. 2A). The thermometer has a diameter of 1 mm, a probe length of 15 mm and belongs to tolerance class A (with an error margin of less than 0.35 °C for measurements below 100 °C) [36]. The measured temperatures were processed and digitized using a resistance-to-digital converter (AX3185, Maxim Integrated, San Jose, USA) [10]. To properly design the temperature flow cell, the following key challenges, must be considered with the

Fig. 2 Overview of the constructed microfluidic sensor flow cells for measuring temperature (**A**), EC (**B**), and pH (**C**). The flow cells were redesigned (**A**, **B**) from subtractive to additive manufacturing. The pH sensor flow cell (**C**) was iteratively adjusted to ensure optimal measurement accuracy by varying the slope of the inner channel and the effective area of the glass membrane contacting the microfluidic channel
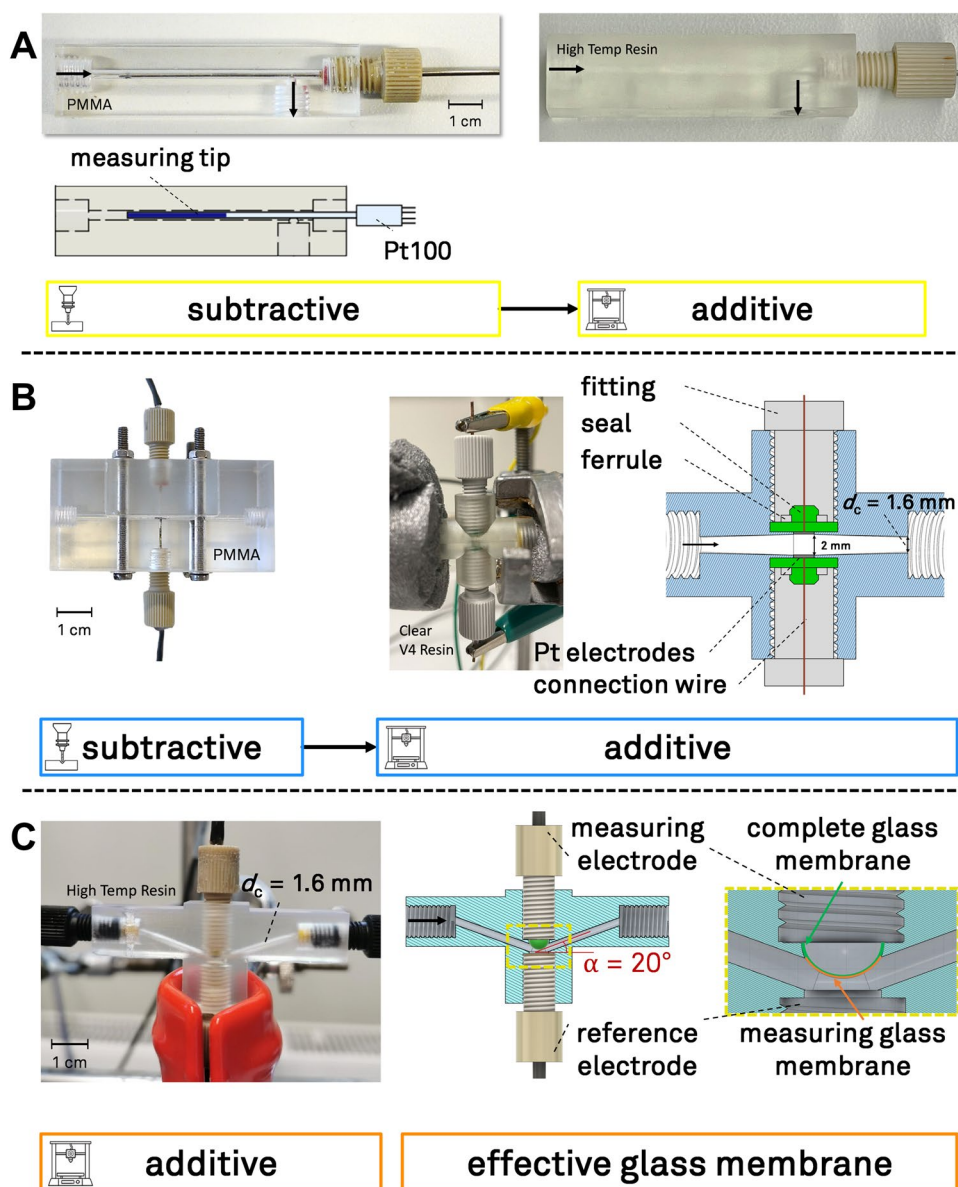
external dimensions and contact area of the Pt100. First, the flow sensor needs to be designed so that the entire measuring tip of the Pt100 was immersed in the fluid to be measured. Since the temperature sensor was placed downstream of the capillary reactor, it was accepted that the temperature sensor would disturb the flow. The sensor design is shown in Fig. 2A and was subtractively manufactured using polymethylacrylate (PMMA), which is optically transparent. The inner channel diameter is 1.6 mm with connecting threads for standard fittings (UNF 1/4" 28G) for easy integration and connection. The temperature sensor flow cell was redesigned for faster iteration of prototypes with higher chemical resistance using additive manufacturing techniques with SL and a photopolymerizing resin.

Electrical conductivity (EC) measurement

The following key challenges must be overcome for the EC flow cell design. First, the disturbances to the flow profile and dead volumes caused by the two immersed platinum (Pt) electrodes must be minimized despite the inline measurement of EC. As shown in the "Electrical conductivity (EC) and conductometry" Section and ESI Section 1, each EC sensor is associated with a cell constant K that should be set to 1 cm^{-1} to ensure universal use and accurate measurements [10, 26, 31]. In order to fulfill these requirements, proposed flow cell designs are shown in Fig. 2B.

First, a subtractive flow cell was designed, consisting of two PMMA parts that are connected during operation and fixed with screws and nuts according to another flow cell design in the literature [1, 8, 18, 37]. The upper and lower parts contain the electrodes, which were inserted coaxially to minimize flow disturbance. The connection threads were fitted with standard fittings (UNF 1/4" 28G), and the inner channel diameter was chosen to be 1.6 mm. This design enables the sensor to be reassembled and the electrodes to be cleaned if necessary. After several months of operation, however, this design reached its limits due to frequent disassembly and reassembly, resulting in leakage and air ingestion that interfered with the measurement of EC. In addition, the permanently soldered electrode plates were difficult to replace, and the chemical resistance of the PMMA flow cell was limited. Consequently, the flow cell was redesigned (Fig. 2B) from subtractive to additive manufacturing as single-part solution using SL 3D printing and the material High Temp and Clear V4 Resin (FLHTAM02, Formlabs GmbH, Berlin, Germany). The new design retains the same inner channel diameter and the Pt electrode material, but the electrode geometry has been changed to planar electrodes to achieve the same cell

constant of $E = 1$ cm^{-1}. The new flow cell design allows that the Pt electrodes can be screwed into the channel via fittings (Fig. 2B).

pH measurement

Analogous to the measurement of EC, the aim of this work was to integrate an open-source glass membrane potentiometric sensor (ENV-10-pH, Atlas Scientific, New York, USA) into a microfluidic flow cell setup to measure temperature-compensated pH value. The microfluidic potentiometric sensor consists of two separate electrodes with standard fittings (UNF 1/4" 28G) to ensure a tight fit in the flow cell. One is the measuring electrode with the green glass sphere as a glass membrane, and the other is the reference electrode, which is fixed in potential between the silver wire and a thin silver chloride film outside the wire.

The following key challenges and external dimensions of the pH sensor must be considered to design the flow cell properly. First, the geometry of the design should avoid the disturbance of air bubbles and entrapped air, and second, the flow cell should also accurately measure the pH value in a microfluidic flow setup. According to the datasheet [38], both electrodes must be immersed in the same solution, whereby the distance between the immersed electrodes is variable and thus represents a degree of freedom for the flow cell design.

However, the electrodes will be relatively close together to avoid using too much material to create the flow cell. Another critical aspect of the flow cell design is the surface area of the glass membrane in contact with the analyte solution, as shown in Fig. 2C. The glass bulb of the measuring electrode has a diameter of 4 mm and a height of 2 mm. This results in a surface area of 28.5 mm^2. This area is too large for the inner channel diameter, resulting in a flow cell where only a percentage of the area is in contact with the analyte solution. The reference electrode has only a small diaphragm at the top center of the electrode that needs to be in contact with the analyte solution. Inserting the glass membrane into the inner channel can disrupt the liquid flow and result in the entrapment of air bubbles around the glass bulb that significantly affects the pH measurement.

In preliminary studies, the flow cell design was iterated to increase the surface area of the pH sensor contacting the analyte solution. The most effective glass membrane area (26.35% of the glass membrane contacting the solution) is shown in Fig. 2C, with an inner channel diameter of 1.6 mm and a 20° inclination of the channel on both sides of the glass membrane. The electrodes were placed opposite each other, 0.6 mm apart, with the measuring electrode at the top and the measuring electrode at the bottom of the flow cell.

Application of sensor flow cells

After the successful development, the model reactions of saponification (ESI Section 5.1) and neutralization (ESI Section 5.2) were conducted to investigate the application scope of the tailored microfluidic sensor flow cells using the experimental setup with the automation strategy of "Experimental setup and automation strategy" Section, ESI Sections 3, and 4. The first application ("Conversion and kinetic parameters of saponification reactions" Section) evaluated the feasibility of calculating the reaction progress and kinetic data for a saponification reaction by measuring temperature-compensated ECs in 25 °C – 35 °C range. In the second application ("Equivalence (pE) and isoelectric (pI) titration points of neutralization reactions" Section), neutralization reactions were conducted, and temperature-compensated pH values were measured to determine if characteristic titration points could be derived from the measurements.

Conversion and kinetic parameters of saponification reactions

The alkaline saponification of ethyl acetate (ESI Section 5.1) was conducted as a model reaction to investigate the microfluidic application of the tailored EC sensor flow cells. The measured ECs were compensated for temperature and normalized to 25 °C. The objective of this study was to evaluate if the conversion (reaction progress) of the model reaction can be calculated based on the temperature-compensated ECs, as they are directly related to the saponification reaction progress, as explained in ESI Section 5.1. Additionally, it was investigated whether the kinetic data of the saponification reaction could be determined from the previously measured data. As initial concentrations, sodium hydroxide (NaOH) and ethyl acetate (EtOAc) were introduced equimolarly with a concentration of 0.05 mol L^{-1}.
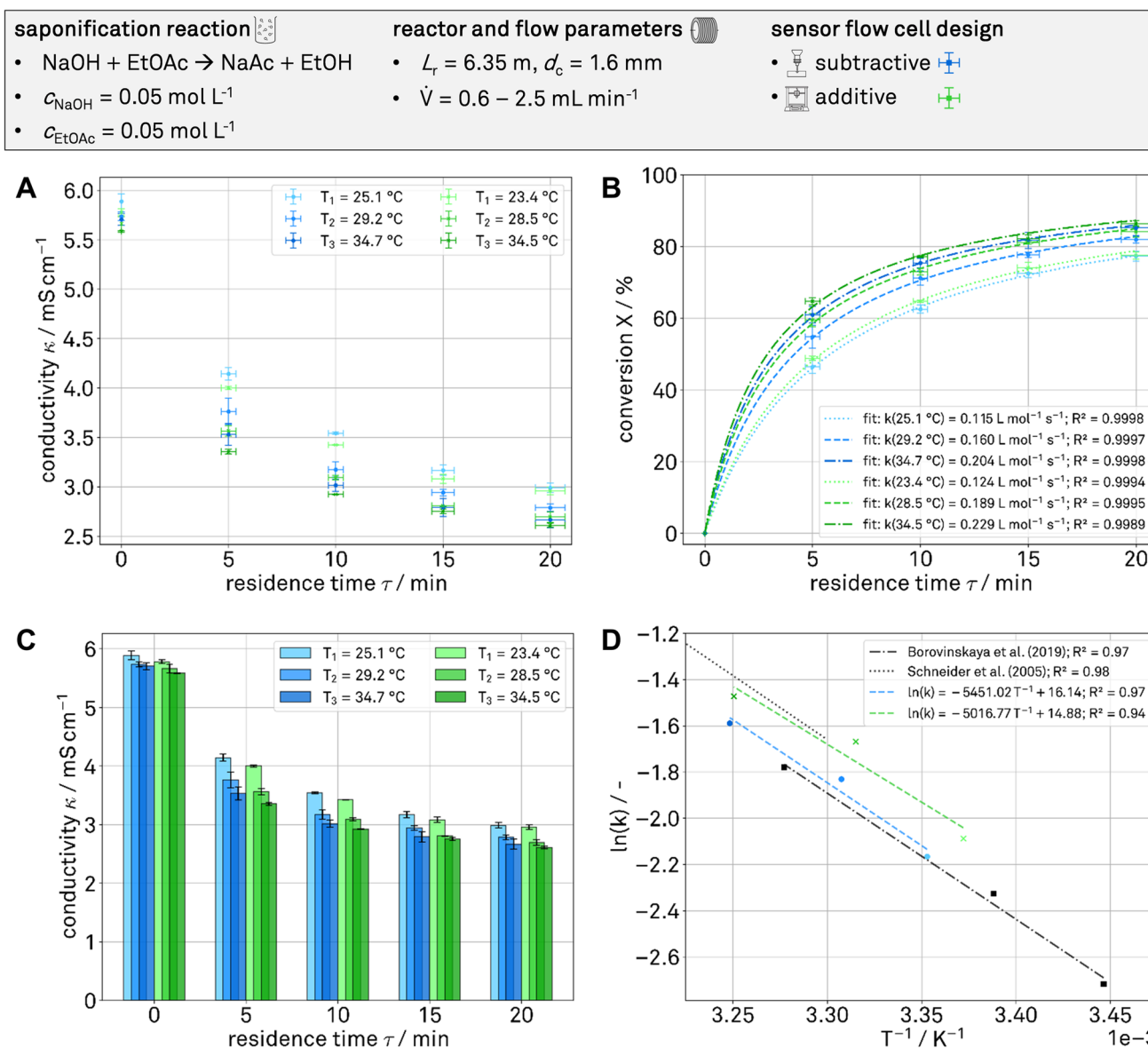
Figure 3A shows the measured EC κ at increasing reaction temperatures (25 °C, 30 °C, 35 °C) using a subtractive (blue) and additive (green) sensor flow cell for increasing residence times τ in the coiled capillary flow reactor. The standard deviation of the measurements is represented by the vertical error bars, while the horizontal error bars indicate the error in the volumetric flow rate of the open-source syringe pumps. As the residence time increases, the measured data decreases as the highly conductive hydroxide (OH$^-$) ions are replaced by the less conductive acetate (Ac$^-$) ions [26]. Additionally, the measured ECs for different residence times are low at high temperatures due to the positive temperature dependence of the rate coefficient k. The measured temperature-compensated ECs are directly related to the conversion of NaOH, as shown in Equation S 8. To determine the rate coefficient k, the kinetic model equation (ESI Section 5.1) is fitted to the experimental data for the NaOH conversion using the least squares method. In Fig. 3B, the representation of the NaOH conversion reveals a reciprocal course compared to the measured EC (Fig. 3A). The conversion starts at approximately 0% and increases to approximately 80% after 20 min. The kinetic models for the conversion sufficiently approximate the experimental data. Moreover, the reaction rate coefficients increased at higher temperatures, as expected from the literature data [39–42]. When comparing the two flow cells, the subtractive and additive flow cells yielded comparable ECs, indicating a successful redesign of the flow cell. To show that the measured EC and approximated rate coefficient of this study are in the same range of the literature data [39–42], the Arrhenius plot (Fig. 3D) was used to derive kinetic data. For the subtractive flow cell, the activation energy E_A is determined to be 45.32 kJ mol^{-1}, and the pre-exponential factor k_0 is $1.02 \bullet 10^7$ L mol^{-1} s^{-1}. The activation energy for the additive flow cell is determined to be 41.71 kJ mol^{-1}, and the pre-exponential factor is $2.89 \bullet 10^6$ L mol^{-1} s^{-1}. These results are summarized in Table S1 and compared with the literature data [39–42], which include the same alkaline saponification of EtOAc with NaOH by measuring the EC in batch by Das *et al.* [40] and Petek *et al.* [41], as well as in flow by Borovinskaya *et al.* [39] and Schneider *et al.* [42]. The activation energy E_A ranges from 41.40 kJ mol^{-1} to 48.00 kJ mol^{-1}, and the pre-exponential factor k_0 ranges from $2.18 \bullet 10^6$ L mol^{-1} s^{-1} to $2.86 \bullet 10^7$ L mol^{-1} s^{-1}, depending on the batch or flow setup in the literature [39–42]. The kinetic data obtained in this study are in the same order of magnitude as those data in the literature [39–42] (Fig. 3D).

As preliminary results, the tailored sensor flow cells provided plausible results for inline monitoring of the saponification reaction, determination of conversions, and kinetic data estimation. This simple and low-effort sensor flow cell concept is comparable to commercial, expensive, complex measurement and calorimeter setups. This feasibility study demonstrates the potential application range, where literature data provides appropriate limits for the performance of the tailored EC sensor flow cells in this work.

Equivalence (pE) and isoelectric (pI) titration points of neutralization reactions

The neutralization reactions (ESI Section 5.2) were conducted to investigate the effectiveness and applicability of the tailored pH sensor flow cell to determine the pE and pI of neutralization reactions. This was accomplished by performing the neutralization while decreasing the volumetric flow rate with increasing pH, as shown in Figure S1 and ESI Section 5.2. The objective of this study was to compare the results obtained from batch and flow titration procedures and to determine the feasibility of the open-source and tailored pH sensor flow cell for precise and accurate pH

saponification reaction
- NaOH + EtOAc → NaAc + EtOH
- $c_{NaOH} = 0.05$ mol L⁻¹
- $c_{EtOAc} = 0.05$ mol L⁻¹

reactor and flow parameters
- $L_r = 6.35$ m, $d_c = 1.6$ mm
- $\dot{V} = 0.6 – 2.5$ mL min⁻¹

**sensor flow cell design**
- subtractive
- additive

Fig. 3 Results and comparison of tailored sensor flow cells (blue: subtractive flow cell, green: additive flow cell) for measuring temperature-compensated electrical conductivities (ECs) of the saponification reaction (**A**, **C**). Calculated conversions from measured temperature-compensated electrical conductivities with fitted curves for the theoretical kinetic models (**B**). Kinetic parameters of the saponification reaction determined by the Arrhenius plot (**D**)

measurements and determination of equivalence and isoelectric titration points (Fig. 4).

In the first set of experiments (Fig. 4A), the batch titration curve (gray) was recorded three times with the corresponding standard deviation (light gray area) and plotted as a function of the degree of titration τ (Fig. 4A). Neutralization started with 50 mL of hydrochloric acid (HCl; 0.1 mol L⁻¹), and 1 mL min⁻¹ NaOH (0.1 mol L⁻¹) was added continuously. The batch titration took 108 min and a total of 108 mL of NaOH was added throughout the titration. In parallel, the experimental flow setup (ESI Section 3.1) was used to transform the titration curve into a

flow experiment. The volumetric flow rate of one pump was kept constant while the volumetric flow rate of the second pump was increased, as described in ESI Section 5.2. Instead of measuring the complete titration curve, stationary points were measured three times (orange points) and the titration curve was interpolated using cubic spline interpolation (orange curve), as shown in Fig. 4A-a). The inflection point of the titration curve represents the pE where the hydrogen and hydroxide ion concentrations are equal, which is theoretically at $\tau = 1$ and $pH = 7$. In the batch measurement, the pE is reached at $pH = 7.1 \pm 0.6$ and in the flow measurement at $pH = 7.42 \pm 1.18$. The titration curves are derived
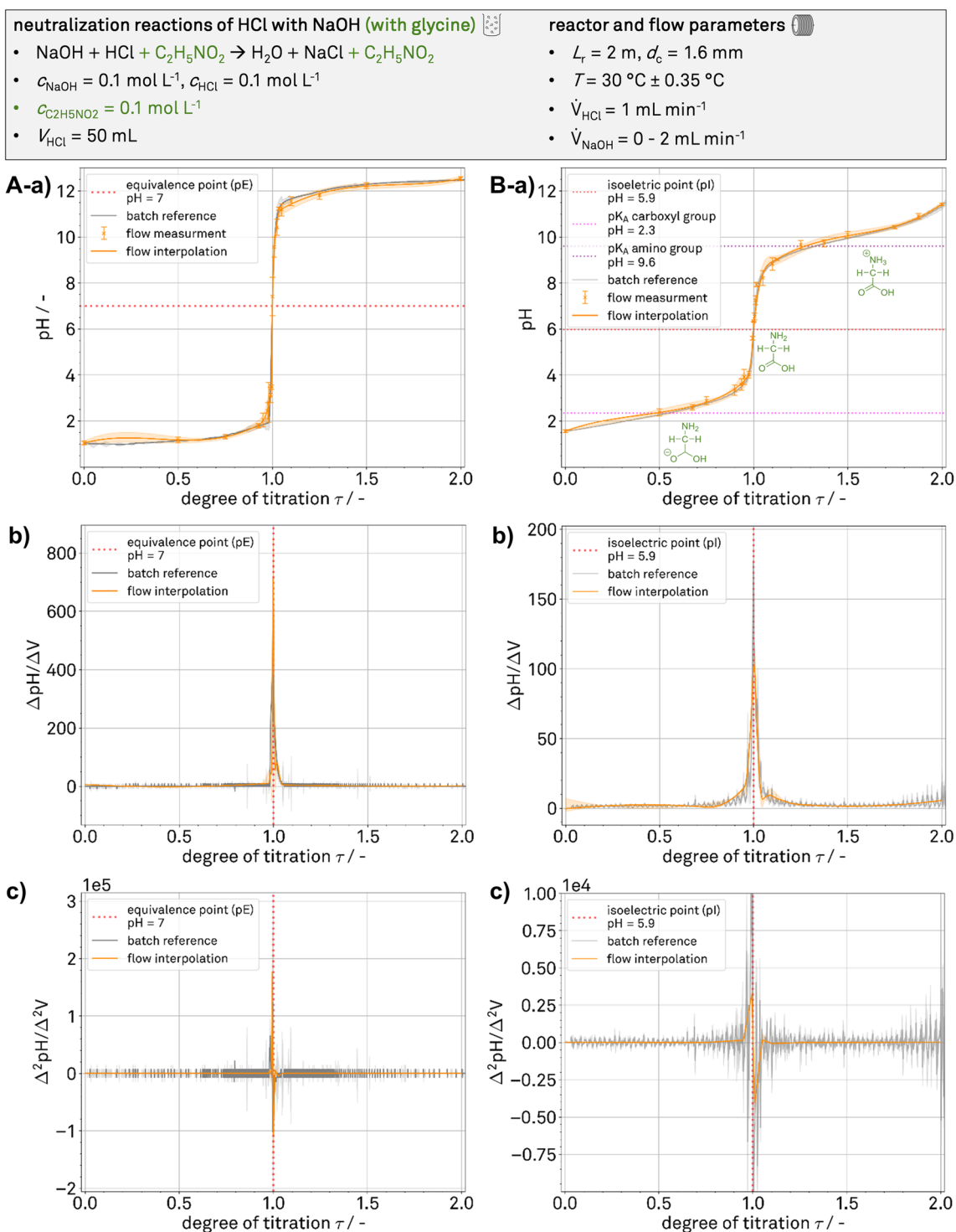
Fig. 4 Results of batch and flow neutralization of HCl with NaOH (**A**) and the same reaction with the amino acid glycine (**B**). Standard titration curves (a) showing the degree of titration after measuring temperature-compensated pH values using the tailored sensor flow cells. First derivative (b) and second derivative (c) titration curves to identify the characteristic equivalence point (pE) and isoelectric point (pI) of the titrations

to investigate whether the tailored microfluidic sensor flow cell is suitable for accurately determining the pE. Looking at the first derivative (Fig. 4A-b) of the titration curve, an

orange peak can be observed at $\tau = 1$. This indicates that it is possible to experimentally determine the pE with the tailored pH sensor flow cell. The result is confirmed by the

second derivative (Fig. 4A-c) of the titration curve, as the pE intersects with the volume x-axis. When comparing batch and flow, the general trend of the titration curve is met, and the flow measurements are set in relation to the measured value of the reference batch potentiometer.

The same neutralization was conducted in a second set of experiments using the amino acid glycine (ESI Section 5.2) as a buffer system (Fig. 4B). This causes glycine to undergo three charge changes during the reaction until it reaches the pI, where the molecule has no net electrical charge, as explained in ESI Section 5.2. The first and second deviations were calculated again to determine the pI and compare batch and flow measurements. As seen in Fig. 4B, the pH sensor flow cell can effectively identify the pI of a more complex neutralization system.

In this advanced application of the tailored pH sensor flow cell, the characteristic points were accurately and precisely detected compared to parallel batch experiments. As preliminary results, it was shown that a neutralization and a more complex reaction with two buffer groups can be accurately monitored with the tailored microfluidic inline pH sensor flow cell. The pE and pI were determined with plausible results using a simple, low-budget, and open-source pH sensor setup comparable to commercial, expensive, and complex measurement setups. This feasibility study demonstrates the potential and limitations of the performance of tailored sensor flow cells and open-source measurement techniques for pH monitoring and determination of characteristic titration points.

Conclusion and outlook

Sensor flow cells for inline temperature, EC, and pH measurements were effectively designed to monitor microfluidic process parameters successfully, utilizing open-source lab automation as a cost-effective tool. By connecting the temperature flow cell to the EC or pH flow cell, linear temperature compensation in the range of 25 °C – 35 °C successfully compensated the measured values. Subtractively manufactured sensor flow cells were successfully adapted and redesigned for additively manufactured (3D-printed) flow cells without losing measurement accuracy and precision. The potential and performance of the newly 3D-printed sensor flow cells were successfully investigated by conducting model reactions in a single-phase capillary flow system, which were compared with a reference batch system. By conducting the saponification reaction of EtOAc with NaOH, the temperature-compensated ECs measured the reaction progress within a 2% error margin for ECs < 10 mS cm^{-1}. The neutralization of HCl with NaOH with glycine as buffer system was conducted and showed reproducible temperature-compensated pH values that met

the theoretical prediction within a 2% error margin typical for flow titration. This facilitated real-time monitoring of reaction progress, determining reaction parameters (conversion, activation energy, and pre-exponential factors), and the quantitative and qualitative identification of titration characteristics (pE and pI). Overall, this study highlights the efficiency and applicability of microfluidic sensor flow cells for accurate and precise inline measurements in capillary flow processes as an alternative to commercial and costly analytical devices.

These promising results will pave the way for a wider range of applications and use-cases, e.g. determine the residence time distribution (RTD) or monitor the alkaline DNA denaturation and stability [43]. Another promising application is the measurement of ECs or pH values at higher process temperatures, enabling further kinetic studies and ensuring accurate measurements at high temperatures. Additionally, scaling down the sensor flow cell from the mL-scale to the μL-scale is an interesting prospect for integration into automated flow chemistry platforms [44].

Abbreviations AC: Alternating voltage; C4D: Capacitively coupled contactless conductivity sensor; csv: Comma-separated-value; EC: Electrical conductivity; EtOAc: Ethyl acetate; FEP: Fluoroethylene propylene; H_2O: Water; HCl: Hydrochloric acid; KCl: Potassium chloride; MCB: Microcontroller board; NaCl: Sodium chloride; NaOH: Sodium hydroxide; pE: Equivalence point; pI: Isoelectric point; PMMA: Polymethylacrylate; Pt: Platinum; RTD: Residence time distribution; SL: Stereolithography

Data Availability The original contributions presented in the study are included in the article, supplementary material and the GitHub repository in the associated content. Further inquiries can be directed to the corresponding authors.

Declarations

Conflict of interest On behalf of all authors, the corresponding authors state that there is no conflict of interest.

References

1. Höving S, Bobers J, Kockmann N (2022) Open-source multi-purpose sensor for measurements in continuous capillary flow. J Flow Chem 12(2):185–196. https://doi.org/10.1007/s41981-021-00214-w

2. Trojanowicz M (2016) Flow chemistry vs. flow analysis. Talanta 146:621–640. https://doi.org/10.1016/j.talanta.2015.07.043

3. Trojanowicz M (2008) Advances in Flow Analysis. Wiley-VCH Verlag, Weinheim, Germany. https://doi.org/10.1002/9783527623259

4. Gioiello A, Moroni G, Cerra B (2022) Integrated systems for continuous synthesis and biological screenings. In: Flow and microreactor technology in medicinal chemistry; methods and principles in medicinal chemistry, pp 159–197. https://doi.org/10.1002/9783527824595.ch5

5. Guidi M, Seeberger PH, Gilmore K (2020) How to approach flow chemistry. Chem Soc Rev 49(24):8910–8932. https://doi.org/10.1039/C9CS00832B

6. Kockmann N (2019) Digital methods and tools for chemical equipment and plants. React Chem Eng 4(9):1522–1529. https://doi.org/10.1039/C9RE00017H

7. Ji H, Li Z, Wang B, Huang Z, Li H, Yan Y (2014) Design and implementation of an industrial C4D sensor for conductivity detection. Sensors Actuators A Phys 213:1–8. https://doi.org/10.1016/j.sna.2014.03.024

8. von Vietinghoff N, Lungrin W, Schulzke R, Tilly J, Agar DW (2020) Photoelectric sensor for fast and low-priced determination of Bi- and triphasic segmented slug flow parameters. Sensors 20(23). https://doi.org/10.3390/s20236948

9. Demori M, Ferrari V, Strazza D, Poesio P (2010) A capacitive sensor system for the analysis of two-phase flows of oil and conductive water. Sensors Actuators A Phys 163(1):172–179. https://doi.org/10.1016/j.sna.2010.08.018

10. Dinter R, Helwes L, Pillath M, Kockmann N (2022) P03 - electrical conductivity sensor with open-source hardware for the microfluidic determination of reaction parameters. In 16. Dresdner Sensor-Symposium 2022, pp 86–90. https://doi.org/10.5162/16dss2022/p03

11. Dinter R, Willems S, Hachem M, Streltsova Y, Brunschweiger A, Kockmann N (2023) Development of a two-phase flow reaction system for DNA-encoded amide coupling. React Chem Eng 8(6):1334–1340. https://doi.org/10.1039/D3RE00020F

12. Au AK, Huynh W, Horowitz LF, Folch A (2016) 3D-printed microfluidics. Angew Chemie Int Ed 55(12):3862–3881. https://doi.org/10.1002/anie.201504382

13. Dinter R, Willems S, Nissalk T, Hastürk O, Brunschweiger A, Kockmann N (2023) Development of a microfluidic photochemical flow reactor concept by rapid prototyping. Front. Chem 11. https://doi.org/10.3389/fchem.2023.1244043

14. Ainla A, Mousavi MPS, Tsaloglou M-N, Redston J, Bell JG, Fernández-Abedul MT, Whitesides GM (2018) Open-source potentiostat for wireless electrochemical detection with smartphones. Anal Chem 90(10):6240–6246. https://doi.org/10.1021/acs.analchem.8b00850

15. Prabhu GRD, Yang T-H, Hsu C-Y, Shih C-P, Chang C-M, Liao P-H, Ni H-T, Urban PL (2020) Facilitating chemical and biochemical experiments with electronic microcontrollers and single-board computers. Nat Protoc 15(3):925–990. https://doi.org/10.1038/s41596-019-0272-1

16. Milanovic JZ, Milanovic P, Kragic R, Kostic M (2018) "Do-it-yourself" reliable PH-stat device by using open-source software, inexpensive hardware and available laboratory equipment. PLoS ONE 13(3). https://doi.org/10.1371/journal.pone.0193744

17. Tu K-H, Yu L-S, Sie Z-H, Hsu H-Y, Al-Jamal KT, Wang JT, Chiang Y-Y (2021) Development of real-time transendothelial electrical resistance monitoring for an in vitro blood-brain barrier system. Micromachines 12(1). https://doi.org/10.3390/mi12010037

18. Glotz G, Kappe CO (2018) Design and construction of an open source-based photometer and its applications in flow chemistry. React Chem Eng 3(4):478–486. https://doi.org/10.1039/C8RE00070K

19. Haber C, Jones W, Soglia J, Surve M, McGlynn M, Caplan A, Reineck J, Krstanovic C (1996) Conductivity detection in capillary electrophoresis – a powerful tool in ion analysis. J Capillary Electrophor 3:1–11

20. Zemann AJ, Schnell E, Volgger D, Bonn GK (1998) Contactless conductivity detection for capillary electrophoresis. Anal Chem 70(3):563–567. https://doi.org/10.1021/ac9707592

21. Fracassi da Silva JA, do Lago CL (1998) An oscillometric detector for capillary electrophoresis. Anal Chem 70(20):4339–4343. https://doi.org/10.1021/ac980185g

22. Harvey D (2000) Modern analytical chemistry. McGraw Hill

23. Magnusson EB, Halldorsson S, Fleming RMT, Leosson K (2013) Real-time optical PH measurement in a standard microfluidic cell culture system. Biomed Opt Express 4(9):1749–1758. https://doi.org/10.1364/BOE.4.001749

24. Naciri M, Kuystermans D, Al-Rubeai M (2008) Monitoring PH and dissolved oxygen in mammalian cell culture using optical sensors. Cytotechnology 57(3):245–250. https://doi.org/10.1007/s10616-008-9160-1

25. aquila biolabs GmbH. Online pH and dissolved Oxygen Monitoring in Flow Loops. https://www.scientificbio.com/flow-cell. Accessed 2023-11-07

26. Atkins P, De Paula J (2006) Atkins' physical chemistry. W. H. Freeman

27. Cosoli G, Mobili A, Tittarelli F, Revel GM, Chiariotti P (2020) Electrical resistivity and electrical impedance measurement in mortar and concrete elements: a systematic review. Appl Sci 10(24). https://doi.org/10.3390/app10249152

28. Baghbani R, Moradi MH, Shadmehr MB, Sanat ZM (2019) A new bio-impedance forceps sensor for measuring electrical conductivity of the biological tissues. IEEE Sens J 19(23):11721–11731. https://doi.org/10.1109/JSEN.2019.2937813

29. Vogt M, Hidalgo S, Musch T, Mallach M, Lange T, Förster J (2019) Concepts for accurate electrical conductivity measurement of liquids in industrial process analytics. Tagungsband. https://doi.org/10.5162/sensoren2019/1.4.3

30. Chaparro CV, Herrera LV, Meléndez AM, Miranda DA (2016) Considerations on electrical impedance measurements of electrolyte solutions in a four-electrode cell. J Phys Conf Ser 687(1):12101. https://doi.org/10.1088/1742-6596/687/1/012101

31. Atlas Scientific. What Are Conductivity Probe Cell Constants? https://atlas-scientific.com/blog/conductivity-probe-cell-constants/. Accessed 2023-11-07

32. Cox BG (2013) Acids and bases: solvent effects on acid-base strength. OUP Oxford

33. Kenkel J (2002) Analytical chemistry for technicians, 3rd ed. CRC Press: Emeritus, Southeast Community College, Lincoln, Nebraska, USA

34. Cheng KL, Chang H (1985) The deviation potential of PH glass electrode. Microchim Acta 85(1):95–101. https://doi.org/10.1007/BF01199932

35. Booeshaghi AS, Beltrame E da V, Bannon D, Gehring J, Pachter L (2019) Principles of open source bioinstrumentation applied to the poseidon syringe pump system. Sci Rep 9(1):12385. https://doi.org/10.1038/s41598-019-48815-9

36. ES Electronic Sensor GmbH. Standard-sheathing resistance thermometer, flexible, Cat. A. https://www.electronic-sensor.de/widerstandsthermometer/standard-biegbar. Accessed 2023-11-07

37. Oliveira M, Conceição P, Kant K, Ainla A, Diéguez L (2021) Electrochemical sensing in 3D cell culture models: new tools for developing better cancer diagnostics and treatments. Cancers (Basel) 13(6). https://doi.org/10.3390/cancers13061381

38. Atlas Scientific. Micro pH Probe #ENV-10-pH. https://atlas-scientific.com/probes/micro-ph-probe/. Accessed 2023-11-07

39. Borovinskaya E, Khaydarov V, Strehle N, Musaev A, Reschetilowski W (2019) Experimental studies of ethyl acetate saponification using different reactor systems: the effect of volume flow rate on reactor performance and pressure drop. Appl Sci 9(3). https://doi.org/10.3390/app9030532

40. Das K, Sahoo P, Sai Baba M, Murali N, Swaminathan P (2011) Kinetic studies on saponification of ethyl acetate using an innovative conductivity-monitoring instrument with a pulsating sensor. Int J Chem Kinet 43(11):648–656. https://doi.org/10.1002/kin.20597

41. Petek A, Krajnc M (2012) The enthalpy and entropy of activation for ethyl acetate saponification. Int J Chem Kinet 44(10):692–698. https://doi.org/10.1002/kin.20712

42. Schneider M-A, Stoessel F (2005) Determination of the kinetic parameters of fast exothermal reactions using a novel microreactor-based calorimeter. Chem Eng J 115(1):73–83. https://doi.org/10.1016/j.cej.2005.09.019

43. Wang X, Lim HJ, Son A (2014) Characterization of denaturation and renaturation of DNA for DNA hybridization. Env Anal Heal Toxicol 29:e2014007. https://doi.org/10.5620/eht.2014.29.e2014007

44. Dinter R, Götte K, Gronke F, Justen L, Brunschweiger A, Kockmann N (2023) Development of an automated flow chemistry affinity-based purification process for DNA-encoded chemistry. J Flow Chem. https://doi.org/10.1007/s41981-023-00282-0

Associated content

The Electronic Supporting Information (ESI) is provided for this article and contains materials, instruments, experimental procedures, and further information on the tailored equipment.

The technical files for 3D printing and the code developed for the microcontroller boards are available in a GitHub repository: https://github.com/TUDoAD/3D-printed-Open-Source-Sensor-Flow-Cells-for-Microfluidic

The repository may be subject to changes due to further contributions. Thus, the state of the repository, as described in this paper, is available on Zenodo: https://doi.org/10.5281/zenodo.10591726